




# Prebiotic aqueous reactions catalyzed by native nickel without hydrogen

Carolina Garcia Garcia , Max Brabender  and William F. Martin 

Institute of Molecular Evolution, Heinrich Heine University Düsseldorf, Germany

## Keywords

hydrogen; hydrothermal vents; native metals; origin of life; origin of metabolism; serpentinization

## Correspondence

C. Garcia Garcia, Institute for Molecular Evolution, Düsseldorf University, Universitätsstrasse 1, 40225 Düsseldorf, Germany

Tel: +49 211 811 2343

E-mail: [garciaga@hhu.de](mailto:garciaga@hhu.de)

(Received 6 January 2026, revised 12 March 2026, accepted 30 March 2026)

doi:10.1111/febs.70556

Compared to iron, nickel is comparatively rare as a transition metal in enzymes. However, it is essential in several enzymes of carbon and energy metabolism in acetogens (bacteria) and methanogens (archaea), which use the acetyl-CoA pathway of H<sub>2</sub>-dependent CO<sub>2</sub> fixation. Nickel containing enzymes of acetogens and methanogens include FeNi hydrogenase, carbon monoxide dehydrogenase, acetyl-CoA synthase and, in methanogens, methyl-CoM reductase in the last step of methane synthesis. Several lines of evidence implicate the acetyl-CoA pathway as the most ancient pathway of CO<sub>2</sub> fixation, most notably recent findings that the overall reaction of the enzymatic pathway from H<sub>2</sub> ( $E_0' = -414$  mV) and CO<sub>2</sub> to pyruvate can be replaced by Ni<sup>0</sup> alone in water as the lone catalyst. Here, we studied Ni<sup>0</sup> as a catalyst and reductant for nonenzymatic redox reactions that require only a mild reductant, as the midpoint potential of Ni<sup>0</sup> oxidation to Ni<sup>2+</sup> is  $E_0' = -260$  mV. We showed that Ni<sup>0</sup> in water can convert 2-oxo acids to 2-hydroxy acids and, in the presence of NH<sub>3</sub>, to amino acids at 25–100 °C without the addition of H<sub>2</sub>, and that it functions as a catalyst and reductant for the fumarate reductase reaction. The findings expand the repertoire of ancient metabolic reactions that Ni<sup>0</sup> can catalyze without proteins, cofactors, or sulfur, shedding light on the broad catalytic activity and substrate specificity of Ni<sup>0</sup> at metabolic origin.

## Introduction

Metabolism is a chemical reaction. It emerged from reactions catalyzed by environments present on the early Earth and gave rise to the metabolic reaction networks of living cells [1–4]. Modern microbes possess enzymes and cofactors that accelerate the reactions of metabolism so that all reactions take place at roughly the same rate [5]. At the very onset of metabolism, there were no enzymes or cofactors, only inorganic catalysts [6]. Transition metals play a crucial role in theories for metabolic origin because they are notoriously good at accelerating particularly difficult chemical reactions such as N<sub>2</sub> reduction [7]. Coordinated in proteins and cofactors, Fe, Ni, Co, and Mo (sometimes replaced by W [8]) are essential to catalysis in

anaerobic autotrophs and are abundant in enzymes of the acetyl-CoA pathway [9–14]. Among pathways of CO<sub>2</sub> fixation, the acetyl-CoA pathway is the most ancient, the only one that occurs in bacteria and archaea [15,16] and the only one that serves both carbon and energy metabolism [13,17]. It is the starting point of metabolism in acetogens (bacteria) and methanogens (archaea) respectively [17,18], and it traces to the last universal common ancestor [19,20].

The most common transition metal in enzymes is Fe, which usually occurs in electron-transferring FeS clusters [21]. As an example, formyl-methanofuran dehydrogenase of the acetyl-CoA pathway in methanogens contains 46 electron-transferring 4Fe4S clusters

## Abbreviations

ACS, acetyl-CoA synthase; CODH, carbon monoxide dehydrogenase; Hyd, hydrogenases; MCR, methyl-CoM reductase; NPN, nickel-pincer nucleotide.

[22]. By contrast, Ni is rarely required by enzymes, and when it occurs, it participates in catalysis at the active site (reviewed by [23,24]). It is found in the active site of (i) urease—the first protein ever crystallized [25]—of (ii) glyoxylase in methylglyoxal detoxification [26], of (iii) acireductone dioxygenase in the methionine salvage pathway [27], and of (iv) Ni-superoxide dismutase [28–30], and in the active site of three enzymes of the acetyl-CoA pathway: In [Fe-Ni] hydrogenases (Hyd), Ni catalyzes the H<sub>2</sub>-dependent reduction of ferredoxin [31–36]. In carbon monoxide dehydrogenase (CODH), Ni catalyzes the reduction of CO<sub>2</sub> to CO [14,34,37–41]. In acetyl-CoA synthase (ACS), Ni catalyzes the synthesis of acetyl-CoA from CO, CoASH and a methyl group [14,34,39,41–42]. In methanogens, nickel in F<sub>430</sub> also catalyzes the final step of methane synthesis at methyl-CoM reductase (MCR) [43–47]. The antiquity CO<sub>2</sub> fixation via the acetyl-CoA pathway [13,17] and the 3.5 Ga age of methanogenesis [48] trace Ni-based catalysis to the onset of biochemical evolution [49].

Although Ni in modern enzymes and cofactors is typically coordinated by sulfur or nitrogen atoms, [24,50] this need not represent the ancestral state of catalytic Ni at origins. Inorganic NiS complexes can catalyze the ACS reaction starting from CO and methyl groups [51]. The reduction of CO<sub>2</sub> using NiS or FeS does not, however, take place unless external potentials of ~1000 mV are applied [52–54], whereby that catalysis is afforded not by metal sulfides, but by native metals that are formed from the sulfides on the electrode during the electrochemical reaction [55]. Without electrodes, pure Ni<sup>0</sup> is an excellent catalyst of CO<sub>2</sub> reduction. In the absence of enzymes, Ni<sup>0</sup> in water catalyzes the H<sub>2</sub>-dependent reduction of CO<sub>2</sub> to the products of the acetyl-CoA pathway—formate, acetate, and pyruvate—in hours to days at 50–100 °C [56]. That is, Ni<sup>0</sup> nanoparticles replace the function of 10 enzymes and 10 cofactors of the acetyl-CoA pathway, which require the activity of 127 enzymes in cells [57]. FeNi alloys and FeCo alloys as well as Fe<sup>0</sup> alone catalyze the same spectrum of reactions as Ni<sup>0</sup> [58–63]. Beyond the reactions of the acetyl-CoA pathway, Ni<sup>0</sup> catalyzes reactions of the reverse TCA cycle and H<sub>2</sub>-dependent reductive aminations of various 2-oxoacids to amino acids [64]. Ni<sup>0</sup> will catalyze the reduction of NADH ( $E_0' = -320$  mV) with H<sub>2</sub> ( $E_0' = -414$  mV) [65,66], and it will reductively aminate pyridoxal to pyridoxamine using H<sub>2</sub> [67], though it will not reduce low potential ferredoxin ( $E_0' = -450$  mV) with H<sub>2</sub>, whereas Fe<sup>0</sup> ( $E_0 = -440$  mV at pH0;  $E_0$  ca. –800 mV) at pH14 [68] will [69].

Native nickel and its alloys are naturally deposited in serpentinizing hydrothermal vents by reduction of divalent metal ions with H<sub>2</sub> generated during the serpentinization process [70–72]. Nickel alloys are implicated in the purely geochemical synthesis of methane [73] that occurs in modern serpentinizing hydrothermal systems [74]. Given that serpentinization has been going on since there was liquid water on Earth [3], nickel-based CO<sub>2</sub> reduction and aminations likely operated before enzymes ever existed and continued to operate during the earliest phases of biochemical evolution as the first enzymes and pathways were arising [64,66,67,69,75–76].

While the utility of Ni in enzymes lies in its ability to readily undergo changes of valence state [9,77], its utility in catalysis of H<sub>2</sub>-dependent reductions of organic compounds lies in its ability to absorb and activate H<sub>2</sub>—a property that has been exploited in organic chemistry for over 100 years [78]. Nickel particles avidly bind H<sub>2</sub> as nickel hydride, Ni–H, at particle surfaces. At 1 atm H<sub>2</sub>, essentially all Ni atoms exposed at the surface of a Ni<sup>0</sup> nanoparticle are occupied as Ni–H hydride [79]. At higher H<sub>2</sub> partial pressures, H diffuses into deeper atom layers as well, and at 30 atm of H<sub>2</sub>, a 2.7 nm diameter Ni nanoparticle can bind up to 3% H<sub>2</sub> by weight [78]. For comparison to natural and biological systems, the effluent of serpentinizing hydrothermal vents contains 1–10 atm H<sub>2</sub> [80], methanogens require only 10<sup>–5</sup>–10<sup>–4</sup> atm H<sub>2</sub> to grow [81], while acetogens require 6·10<sup>–5</sup>–10<sup>–3</sup> atm H<sub>2</sub>, depending on the strain [82]. Ni–H formation from Ni<sup>0</sup> and H<sub>2</sub> is both spontaneous and facile [79], yet it is not a redox reaction, as both Ni and H remain in their elemental state. Like Co [83,84], Mo [85,86], and Fe [87,88] nickel also occurs in cofactors: the Ni-tetrapyrrole F<sub>430</sub> of methanogens and in the nickel-pincer nucleotide (NPN) cofactor [89] first described in lactate racemase [90].

The midpoint potential of Ni<sup>0</sup> oxidation to Ni<sup>2+</sup> under physiological conditions is  $E_0' = -260$  mV, sufficient to reduce a number of common biological substrates, for example pyruvate to lactate ( $E_0' = -190$  mV) in the absence of H<sub>2</sub>. With rare exceptions [67], the use of Ni<sup>0</sup> in experimental reconstructions of metabolic origin so far has focused on H<sub>2</sub>-dependent reductions. Here we investigate reactions relevant to prebiotic chemistry using Ni<sup>0</sup> as catalyst and reductant.

## Results

In the presence of H<sub>2</sub>, nickel supplied as commercial nickel silicate powder (Ni-SiO<sub>2</sub>/Al<sub>2</sub>O<sub>3</sub>) catalyzes the



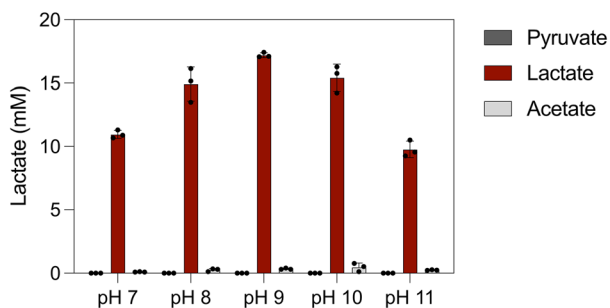


**Fig. 2.** Effect of pH on lactate synthesis in the presence of nickel catalyst. Initial concentrations were 20 mM of pyruvate. Ni-SiO<sub>2</sub>/Al<sub>2</sub>O<sub>3</sub> (1 mmol of Ni atoms) was added as solid phase powder in a total reaction volume of 1.5 mL. The pH was set to 7, 8, 9, 10, and 11 with KOH, respectively, and the reaction time was set to 2 h. The reaction was performed under a 5 bar Ar atmosphere. No H<sub>2</sub> was added. Each dot represents a single measurement. Dots positioned on the X-axis represent measurements where no concentration could be detected. Error bars in the figure indicate standard deviation (SD). Reactions were performed in triplicates.

also tested the possibility of nickel performing double bond reductions. After 2 h at pH 9, fumarate was reduced to succinate ( $E_0' = -130$  mV) with a 100% conversion rate (Fig. 6A; Table S6) The reduction of 2-oxoglutarate to 2-hydroxyglutarate ( $E_0' = -337$  mV) had a 100% conversion, the reduction of 4-methyl-2-oxopentanoate to hydroxyisocaproate ( $E_0' = -344$  mV) was 97% complete after 2 h, while the reduction of 3-methyl-2-oxopentanoate to 2-hydroxy-3-methylvalerate ( $E_0' = -357$  mV) underwent 64% conversion (Fig. 6B–D; Table S6).

We investigated the reductive amination of these alpha-ketoacids to their corresponding amino acids using ammonium, with nickel as the reductant, adjusting the length of the reaction time (72 h) and the pH (pH 11) to improve yields. Under these conditions, nickel has a lower midpoint potential [96], allowing for the reductive amination of the respective compounds. We observed that 4-methyl-2-oxopentanoate underwent reductive amination to leucine ( $E_0' = -386$  mV) with 6.6%

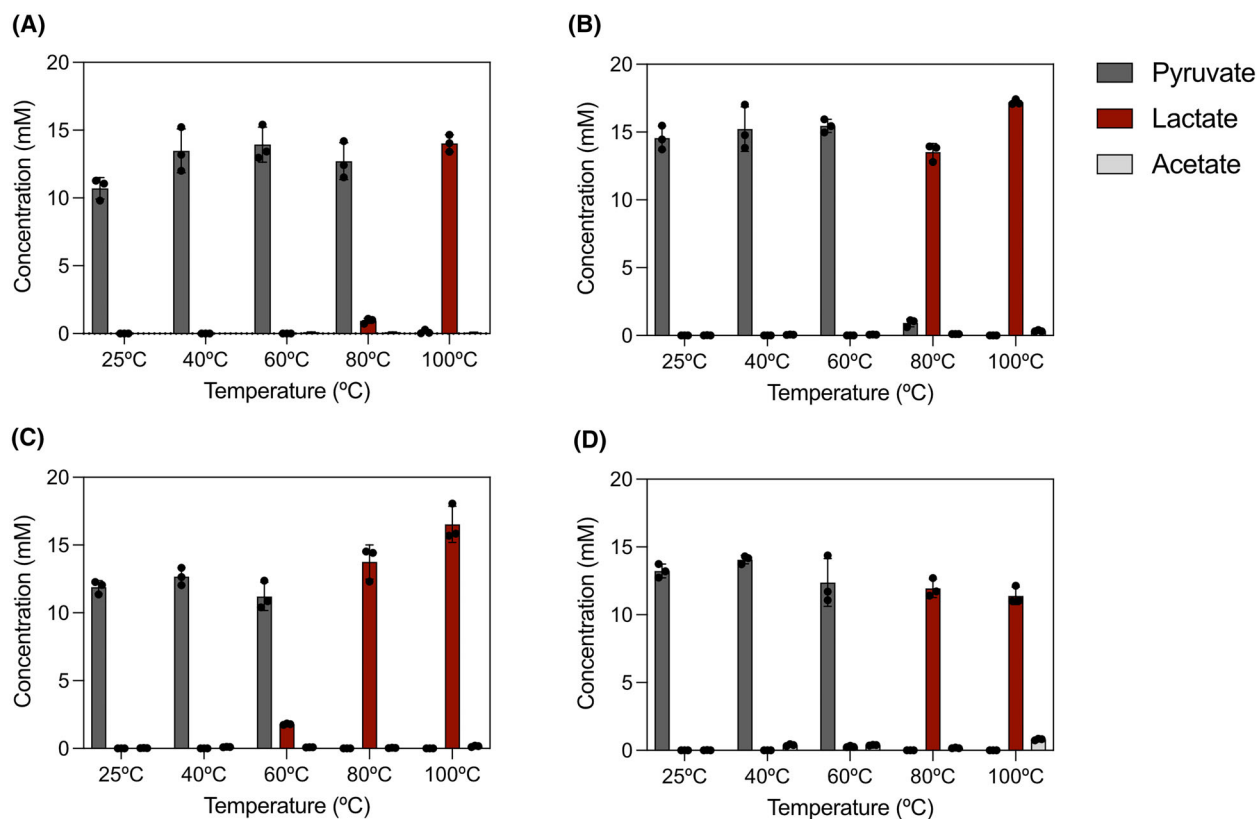


**Fig. 3.** Effect of temperature and time on lactate synthesis in the presence of nickel catalyst. Initial concentrations were 20 mM of pyruvate. Ni-SiO<sub>2</sub>/Al<sub>2</sub>O<sub>3</sub> (1 mmol of Ni atoms) was added as solid phase powder in a total reaction volume of 1.5 mL. The reaction time was 1 h (A), 2 h (B), 4 h (C), and 18 h (D), respectively. Temperature was 25, 40, 60, 80, and 100 °C. The pH was set to 9 with KOH. The reaction was performed under a 5 bar Ar atmosphere. No H<sub>2</sub> was added. Error bars in the figure indicate standard deviation (SD). Reactions were performed in triplicates.

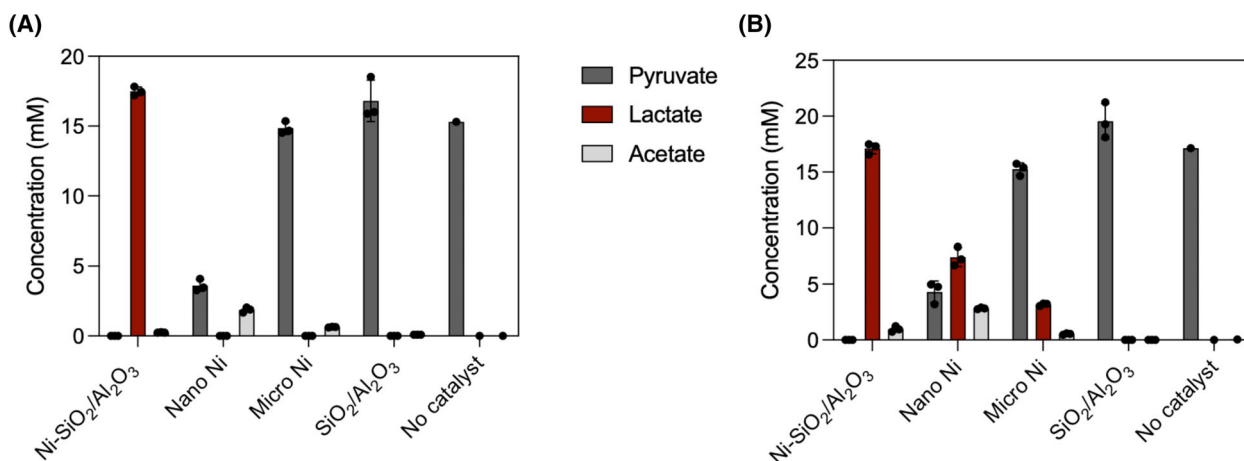


**Fig. 4.** Effect of different catalysts on lactate synthesis. Pyruvate concentration was set to 20 mM. The catalysts (Ni-SiO<sub>2</sub>/Al<sub>2</sub>O<sub>3</sub>, Nano nickel powder, micro nickel powder, SiO<sub>2</sub>/Al<sub>2</sub>O<sub>3</sub>) were added as 1 mmol of Ni atoms of undissolved solid phase powder in a total reaction volume of 1.5 mL. The reaction was performed at 100°C under a 5 bar argon atmosphere; pH was set to 9 with KOH. No H<sub>2</sub> was added. The reaction time was set to 2 h (A) and 18 h (B). Error bars in the figure represent standard deviation (SD). Each reaction was performed in triplicates.

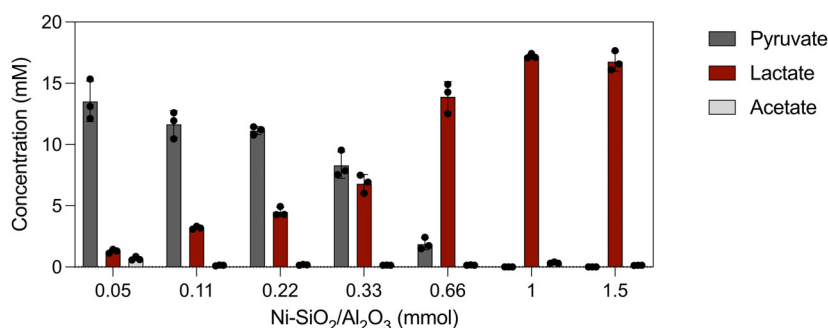


**Fig. 5.** Effect of catalyst concentration on lactate synthesis in the presence of nickel catalyst. Initial concentrations were 20 mM of pyruvate. Ni-SiO<sub>2</sub>/Al<sub>2</sub>O<sub>3</sub> was added as solid phase at a concentration of 0.05, 0.11, 0.22, 0.33, 0.66, 1, and 1.5 mmol of Ni atoms, respectively. The pH was 9 (KOH), and the reaction was performed for 2 h at 100°C, under a 5 bar Ar atmosphere. No H<sub>2</sub> was added. Error bars in the figure represent standard deviation (SD). Each reaction was performed in triplicates.

conversion rate and 3-methyl-2-oxopentanoate was reductively aminated to isoleucine ( $E_0' = -419$  mV) with a 4.8% conversion rate (Fig. 7A,B; Table S7). Reductive amination of 2-oxoglutarate did not generate glutamate ( $E_0' = -380$  mV) but its cyclic peptide derivative 5-oxoproline, which is known to occur at high temperature and high pH [97]. The formation of 5-oxoproline indicates reductive amination to 2-oxoglutarate at 57% (Fig. 7C; Table S7).

## Discussion

Serpentinizing hydrothermal systems are interesting sites for the origin of metabolism because they generate a constant supply of H<sub>2</sub> for CO<sub>2</sub> reduction

[49,98–99] and because there is broad congruence between reactions catalyzed under hydrothermal conditions and reactions of metabolism [19,97]. The process of serpentinization furthermore generates highly alkaline effluent, pH 9–12, producing strongly reducing conditions with potentials on the order of  $-800$  mV or more [90], which are sufficient to reduce divalent metals to native metals [70,72,100–103]. Native metals deposited in serpentinizing hydrothermal vents include Fe, Co, Ni, Pd, other platinum group elements (PGE) and their alloys [70,103–105]. These metals activate H<sub>2</sub> via chemisorption and catalyze organic reactions [60–63] under conditions conducive to the origin of metabolism. A number of recent studies have shown that Ni<sup>0</sup> can promote the conversion of CO<sub>2</sub> to

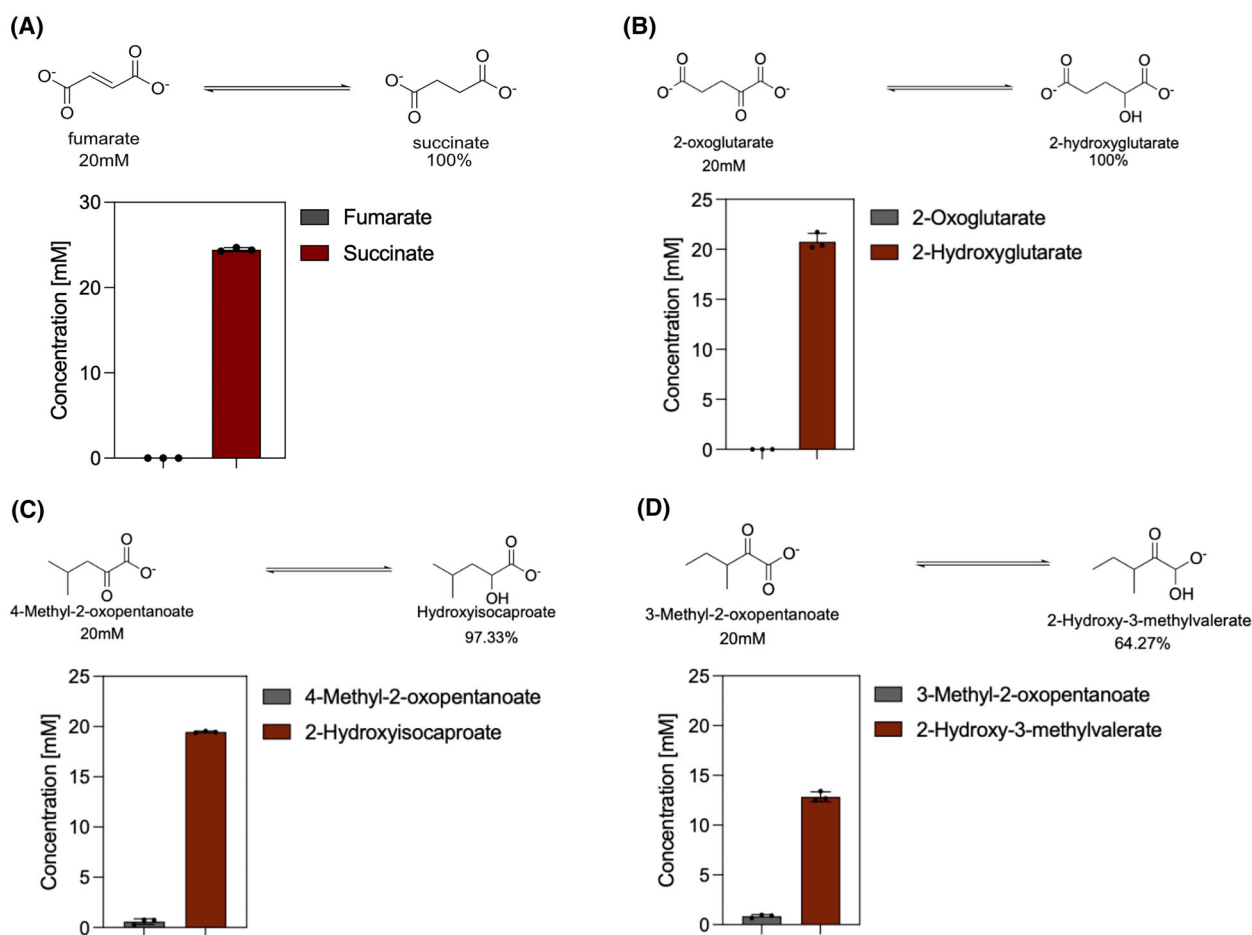


**Fig. 6.** Ketone and double bond reduction in the presence of nickel catalyst. Educt concentration was set to 20 mM. Ni-SiO<sub>2</sub>/Al<sub>2</sub>O<sub>3</sub> (1 mmol of Ni atoms) was added as solid phase powder in a total reaction volume of 1.5 mL. The reaction time was set to 2 h at 100 °C, and pH was set to 9 with KOH. The reaction was performed under a 5 bar Ar atmosphere. No H<sub>2</sub> was added. Error bars in the figure represent standard deviation (SD). Each reaction was performed in triplicates. (A) Succinate synthesis from fumarate. (B) 2-Hydroxyglutarate synthesis from 2-oxoglutarate. (C) 2-Hydroxyisocaproate synthesis from 4-methyl-2-oxopentanoate. (D) 2-Hydroxy-3-methylvalerate synthesis from 3-methyl-2-oxopentanoate.

organic acids using H<sub>2</sub> as the reductant [60,62–63], retracing rather exactly the reactions of the acetyl-CoA pathway [60,62–63] and reactions of the reverse TCA cycle [58,64,106]. In water, Ni<sup>0</sup>, Fe<sup>0</sup> and Co<sup>0</sup> are furthermore compatible with cofactors, catalyzing the H<sub>2</sub> dependent reduction of NAD<sup>+</sup> [65,66], while Ni<sup>0</sup> efficiently catalyzes the H<sub>2</sub> dependent reduction of pyridoxal [67], and Fe<sup>0</sup> catalyzes the reduction of 4Fe4S clusters in ferredoxin [69]. With a midpoint potential of 440 mV, Fe<sup>0</sup> can, and does, generate H<sub>2</sub> in water, and can reduce CO<sub>2</sub> without additional reductants [60]. But Ni<sup>0</sup> ( $E_0' = -270$  mV) is a milder reductant.

Here we have shown that under serpentinizing conditions (high pH, temperature 50–100 °C) Ni<sup>0</sup> can serve as a catalyst and reductant for reduction of

2-oxo groups to hydroxyl, reduction of double bonds, and reductive amination of 2-oxo acids to amino acids. These findings underscore the broad compatibility of native Ni with metabolic reactions. In modern metabolism, Ni is usually coordinated by S, C and N ligands in enzymes and cofactors as the divalent ion, but can undergo valence state changes during enzymatic reactions [23,24,45]. The extremely broad range of biochemical reactions that Ni<sup>0</sup> can catalyze with or without H<sub>2</sub> as a reductant and their similarity, often identical, to the reactions of metabolism in terms of reactants and products indicate that Ni<sup>0</sup> was involved in metabolic origin, as outlined in Fig. 8A–I.

Yet if Ni<sup>0</sup> is so effective as a catalyst, one might ask why is Ni<sup>0</sup> not used as a catalyst by enzymes or cofactors in modern metabolism. Cells can easily generate

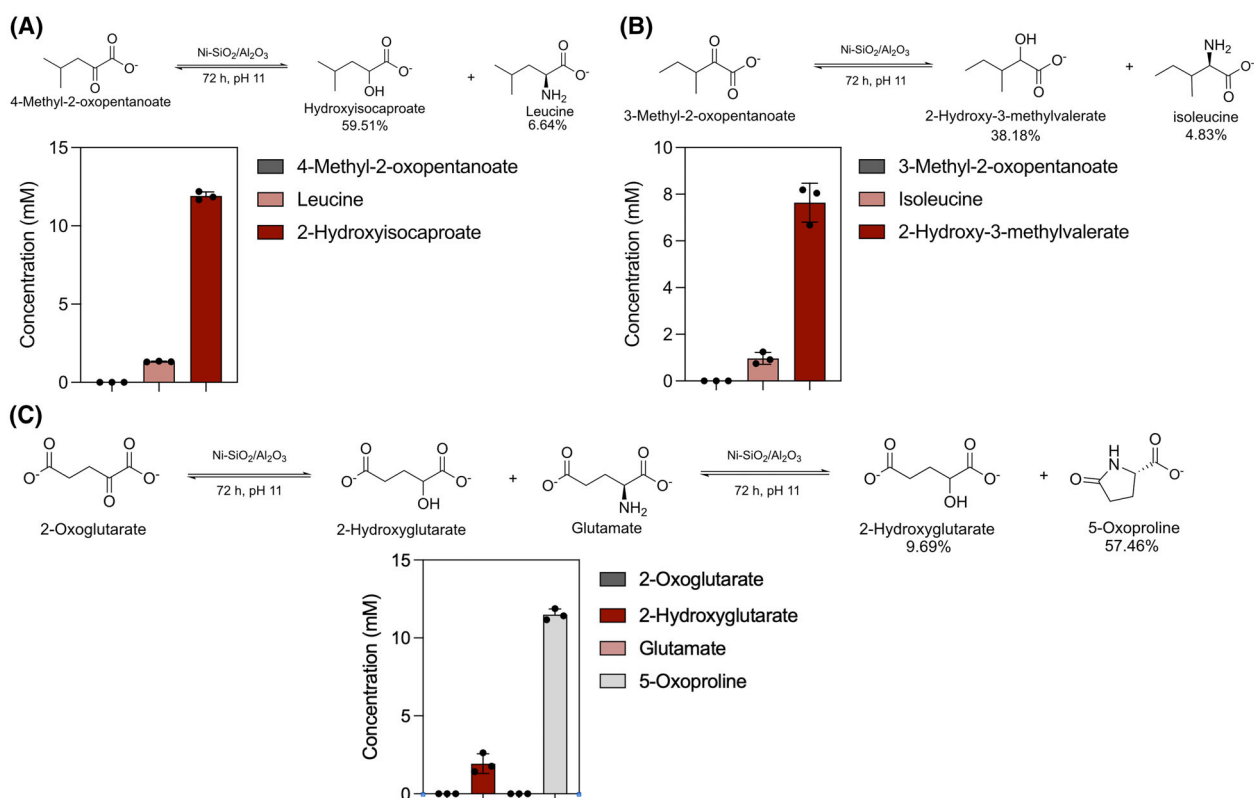


**Fig. 7.** Reductive amination in the presence of nickel catalyst. Initial concentrations were 20 mM of each respective educt and 200 mM ammonium chloride. Ni-SiO<sub>2</sub>/Al<sub>2</sub>O<sub>3</sub> (1 mmol of Ni atoms) was added as solid phase powder in a total reaction volume of 1.5 mL. The reaction was performed under a 5 bar Ar atmosphere, initial pH 11 with KOH, the reaction was set at 72 h and 100 °C. No H<sub>2</sub> was added. Error bars in the figure indicate standard deviation (SD). Reactions were performed in triplicates. (A) Leucine synthesis from 4-methyl-2-oxopentanoate. (B) Isoleucine synthesis from 3-methyl-2-oxopentanoate. (C) 5-Oxoproline synthesis from 2-oxoglutarate.

the potential needed to convert Ni<sup>2+</sup> to Ni<sup>0</sup>, with the help of low potential reduced ferredoxin ( $E_o = -450$  mV) [109] or using H<sub>2</sub> with electron bifurcation [110]. Why is Ni<sup>0</sup> not used by metabolism in cells?

The answer, we suggest, is specificity. Broad substrate specificity is a classical trait of ancient enzymes [111,112]. The first enzymes likely had very broad substrate specificity for a given kind of reaction (reductive amination for example) and diversified into ancient enzyme families each with greater substrate specificity, so that the reactions of (proto-) metabolism proceeded along orderly and well-defined lines. Native nickel is a highly effective catalyst, but catalyzes *too many* different kinds of reactions (Fig. 8A–I). Ni<sup>0</sup> catalyzes H<sub>2</sub> activation (Fig. 8B) [60,62,67] as in hydrogenases [32–36] and CO<sub>2</sub> reduction (Fig. 8D) to formate, acetate, and pyruvate [60,62] including the formation of C–C bonds [60,62–64] as in the acetyl-CoA pathway (Fig. 8H) [17,60]. It catalyzes reactions of the rTCA cycle [58,64,106]. And, as shown here, Ni<sup>0</sup> catalyzes keto to alcohol reductions (Fig. 8I), reductive

transaminations (Fig. 8A), and the reduction of double bonds in the absence of additional reductants (Fig. 8C). All of those reactions take place in water across a broad neutral to alkaline pH range and a wide range of biologically relevant temperatures. The extremely broad substrate specificity of Ni<sup>0</sup> would make it an uncontrolled catalyst in a regulated metabolism, as cells could not turn it off. In a cytosol full with hundreds of metabolites present in μM to mM concentrations, Ni<sup>0</sup> would have no choice but to react with whatever reactive moiety came along first. The utility of Ni<sup>0</sup> in prebiotic biochemical synthesis—capable of performing dozens of different reactions with CO<sub>2</sub>, NH<sub>3</sub>, H<sub>2</sub> and organic moieties—is its liability in regulated metabolism. The catalytic versatility of Ni<sup>0</sup> was likely useful in generating organic molecules at origins, but detrimental as enzymatic metabolism reached a state resembling that of modern cells. In order for natural selection in biochemical evolution to take place, enzymes had to be in control of the reactions they catalyzed. That was possible with Ni<sup>2+</sup>

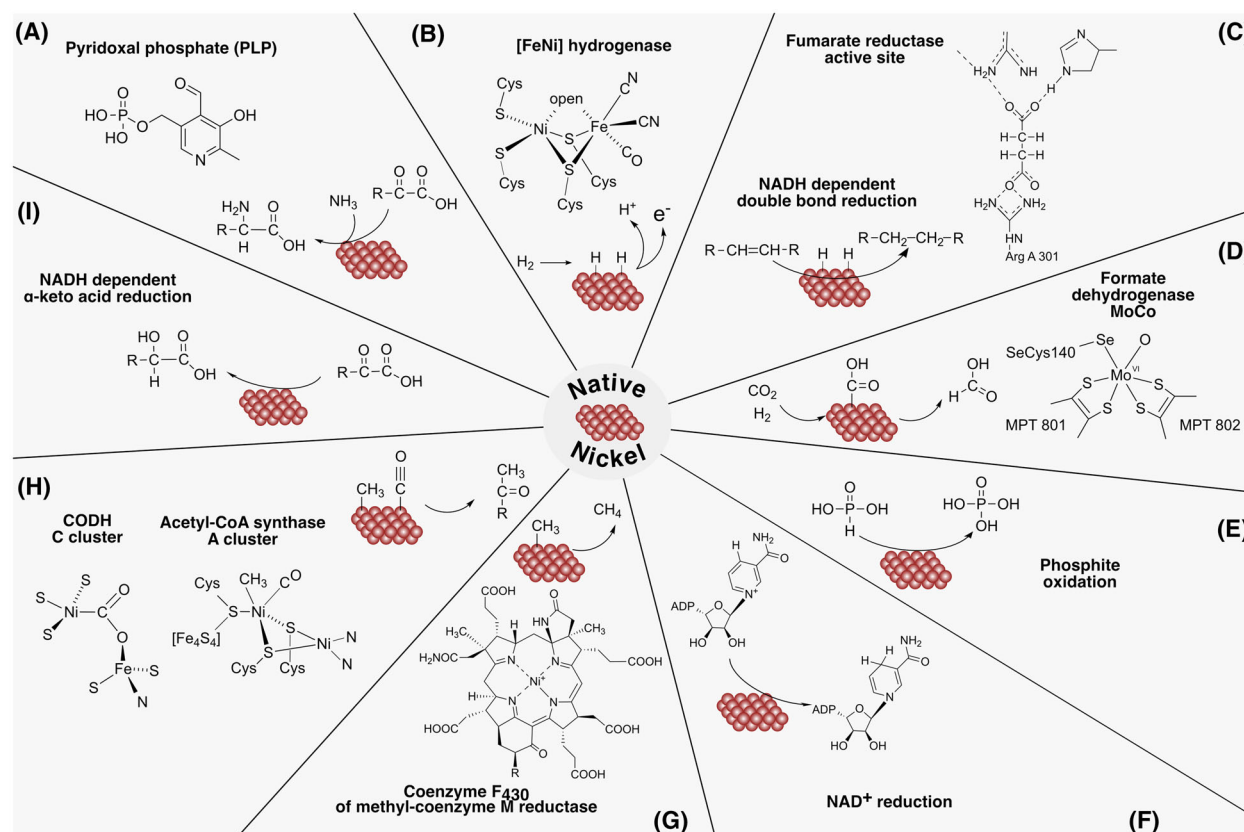


**Fig. 8.** Broad substrate specificity of nickel as a primordial catalyst in metabolism. (A) Reductive amination: the presence of pyridoxal improves the yield [67], but the reaction also proceeds in the presence of Ni<sup>0</sup> alone (this paper). (B) H<sub>2</sub> oxidation: structure of carbon-Ni bond present in [FeNi] hydrogenase [31,32]. Ni<sup>0</sup> activates H<sub>2</sub> [60] (C) Double bond reduction: active site of fumarase taken from [107], the presence of Ni<sup>0</sup> alone catalyzes the reaction (this paper). (D) CO<sub>2</sub> fixation: structure of molybdenum cofactor of formate dehydrogenase [108]; Ni<sup>0</sup> catalyzes the reaction under hydrothermal vent conditions [60]. (E) Phosphite oxidation [97]. (F) NAD<sup>+</sup> reduction [65,66]. (G) Methane formation: Ni<sup>0</sup> generates methane from H<sub>2</sub> and CO<sub>2</sub> [76], the biological reaction requires coenzyme F<sub>430</sub> in methyl-coenzyme M reductase [43]. (H) CO<sub>2</sub> fixation: structure of the carbon-Ni bonds present in carbon monoxide dehydrogenase [37–40], and acetyl-CoA synthase A-cluster [39–42]; Ni<sup>0</sup> catalyzes acetyl synthesis under hydrothermal vent conditions [60]. (I)  $\alpha$ -keto acid reduction: catalyzed by nickel (this paper).

coordinated by N, S, and C in enzymes and cofactors [24] (Fig. 8B,G,H), but not with Ni<sup>0</sup>, which is likely why it was left behind when metabolism escaped the hydrothermal environment [49,97] within which it arose.

## Material and methods

### Reaction conditions

Each reaction contained 20 mM of pyruvate (Sigma-Aldrich), or of its respective educt (2-oxoglutarate, 3-methyl-2-oxopentanoate, 4-methyl-2-oxopentanoate, fumarate; Sigma-Aldrich); and ammonium chloride when needed, dissolved in HPLC grade water (VWR International, Germany). The pH was adjusted from 7 to 11,

depending on the experimental conditions required, by adding 1 M KOH. Ni<sub>2</sub>-Al<sub>2</sub>O<sub>3</sub> (Sigma-Aldrich) was used as a catalyst, added in a concentration between 0.0 mM to 1.5 mM, depending on the experimental conditions required, per mL of reaction volume, with a final reaction volume of 1.5 mL. Samples were prepared in glass vials (5 mL, Rotilabo-Rollr ndfl schen ND20, Roth) and closed with metal lids (VWR International, Germany). Lids were punctured before being placed inside the reactor (Berghoff BR-300 with BTC-3000 temperature controller) to allow for gas exchange. Reactors were filled with 5-bar argon (99.996%; Messer, Switzerland). Reactions were performed at 25, 40, 60, 80 or 100 °C over 1, 2, 4, 18 or 72 h while stirring at 650 × g.

When the reactions were over, reactors were depressurized and the reaction contents were transferred to 2 mL Eppendorf tubes, and centrifuged for 15 min at 13,000 × g

(Biofuge Fresco, Heraeus) to separate the reaction phases (metal contents and supernatant). The supernatants were then analyzed by NMR.

### Product identification

To prepare the samples for NMR analysis, 600 µL of each sample were transferred into NMR tubes (VWR International, Germany). As a reference for calibration, DSS (2,2-dimethyl-2-silapentane-5-sulfonate) was added, reaching a final concentration of 1 mM. NMR spectra were measured on a Bruker Avance III—600 MHz spectrometer by the Center for Molecular and Structural Analytics at Heinrich Heine University Düsseldorf. Spectra were analyzed using Chenomx NMR Suite Version 9.02 software.

### Acknowledgements

This project has received funding from the European Research Council (ERC) under the European Union's Horizon 2020 research and innovation program (grant agreement no. 101018894). For funding, WFM thanks the ERC (101018894), the Deutsche Forschungsgemeinschaft (MA 1426/21-1) and the Volkswagen Foundation (Grant 96\_742). We thank the Center for Molecular and Structural Analytics, Heinrich Heine University (CeMSA@HHU) for recording the NMR-spectroscopic data. We thank Joseph Moran, Harun Tüysüz, and Mirko Basen for many helpful discussions. Open Access funding enabled and organized by Projekt DEAL.

### Conflict of interest

The authors declare no conflict of interest.

### Author contributions

CGG, MB, and WFM designed the research. CGG performed the experiments. CGG, MB, and WFM interpreted and analyzed the data. CGG and WFM visualized the data. CGG, MB and WFM wrote the paper. CGG, MB, and WFM edited the paper.

### Peer review

The peer review history for this article is available at <https://www.webofscience.com/api/gateway/wos/peer-review/10.1111/febs.70556>.

### Data availability statement

The data that supports the findings of this study are available in (Figs 1–7) and the [Supporting Information](#)

of this article. Any raw data not specifically shown in the paper will be available upon request.

### References

- Lipmann F (1965) Projecting backward from the present stage of evolution of biosynthesis. In *The Origins of Prebiological Systems and of Their Molecular Matrices* (Fox SW, ed.), pp. 259–280. Academic Press, New York, NY.
- Baross JA & Hoffman SA (1985) Submarine hydrothermal vents and associated gradient environments as sites for the origin and evolution of life. *Orig Life Evol Biosph* **15**, 327–345.
- Sleep NH, Bird DK & Pope EC (2011) Serpentine and the dawn of life. *Philos Trans R Soc Lond B Biol Sci* **366**, 2857–2869.
- Stüeken EE, Buick R, Guy BM & Koehler MC (2015) Isotopic evidence for biological nitrogen fixation by molybdenum-nitrogenase from 3.2 Gyr. *Nature* **520**, 666–669.
- Wolfenden R & Snider MJ (2001) The depth of chemical time and the power of enzymes as catalysts. *Acc Chem Res* **34**, 938–945.
- Eakin RE (1963) An approach to the evolution of metabolism. *Proc Natl Acad Sci U S A* **49**, 360–366.
- Hu Y & Ribbe MW (2016) Nitrogenases—a tale of carbon atom(s). *Angew Chem Int Ed* **55**, 8216–8226.
- Szaleniec M & Heider J (2025) Obligately tungsten-dependent enzymes—catalytic mechanisms, models and applications. *Biochemistry* **64**, 2154–2172.
- Ragsdale SW & Wood HG (1991) Enzymology of the acetyl-CoA pathway of CO<sub>2</sub> fixation. *Crit Rev Biochem Mol Biol* **26**, 261–300.
- Drennan CL, Doukov TI & Ragsdale SW (2004) The metalloclusters of carbon monoxide dehydrogenase/acetyl-CoA synthase: a story in pictures. *J Biol Inorg Chem* **9**, 511–515.
- Svetlitchnaia T, Svetlitchnyi V, Meyer O & Dobbek H (2006) Structural insights into methyltransfer reactions of a corrinoid iron-sulfur protein involved in acetyl-CoA synthesis. *Proc Natl Acad Sci U S A* **103**, 14331–14336.
- Shima S, Pilak O, Vogt S, Schick M, Stagni MS, Meyer-Klaucke W, Warkentin E, Thauer RK & Ermler U (2008) The crystal structure of [Fe]-hydrogenase reveals the geometry of the active site. *Science* **321**, 572–575.
- Fuchs G (2011) Alternative pathways of carbon dioxide fixation: insights into the early evolution of life? *Annu Rev Microbiol* **65**, 631–658.
- Yin MD, Lemaire ON, Rosas Jiménez JG, Belhamri M, Shevchenko A, Hummer G, Wagner T & Murphy BJ (2025) Conformational dynamics of a multienzyme

- complex in anaerobic carbon fixation. *Science* **387**, 498–504.
- 15 Berg IA, Kockelkorn D, Ramos-Vera WH, Say RF, Zarzycki J, Hügler M, Alber BE & Fuchs G (2010) Autotrophic carbon fixation in archaea. *Nat Rev Microbiol* **8**, 447–460.
  - 16 Berg IA (2011) Ecological aspects of the distribution of different autotrophic CO<sub>2</sub> fixation pathways. *Appl Environ Microbiol* **77**, 1925–1936.
  - 17 Martin WF (2020) Older than genes: the acetyl CoA pathway and origins. *Front Microbiol* **11**, 817.
  - 18 Fuchs G & Stupperich E (1985) Evolution of autotrophic CO<sub>2</sub> fixation. In *Evolution of Prokaryotes* (Schleifer KH & Stackebrandt E, eds), pp. 235–251. Academic Press, London.
  - 19 Weiss MC, Sousa FL, Mrnjavac N, Neukirchen S, Roettger M, Nelson-Sathi S *et al.* (2016) The physiology and habitat of the last universal common ancestor. *Nat Microbiol* **1**, 1–8.
  - 20 Moody ERR, Álvarez-Carretero S, Mahendrajah TA, Clark JW, Betts HC, Dombrowski N, Szánthó LL, Boyle RA, Daines S, Chen X *et al.* (2024) The nature of the last universal common ancestor and its impact on the early earth system. *Nat Ecol Evol* **8**, 1654–1666.
  - 21 Lovenberg W, Buchanan BB & Rabinowitz JC (1963) Studies on the chemical nature of clostridial ferredoxin. *J Biol Chem* **238**, 3899–3913.
  - 22 Wagner T, Ermler U & Shima S (2016) The methanogenic CO<sub>2</sub> reducing-and-fixing enzyme is bifunctional and contains 46 [4Fe-4S] clusters. *Science* **354**, 114–117.
  - 23 Ragsdale SW (2009) Nickel-based enzyme systems. *J Biol Chem* **284**, 18571–18575.
  - 24 Neubeck A & Kirschning A (2026) Nickel: geochemistry, biochemistry and its role in chemical and biological evolution. *Earth Sci Rev* **272**, 105324.
  - 25 Sumner JB (1926) The isolation and crystallization of the enzyme urease: preliminary paper. *J Biol Chem* **69**, 435–441.
  - 26 Clugston SL, Barnard JFJ, Kinarch R, Miedema D, Ruman R, Daub E *et al.* (1998) Overproduction and characterization of a dimeric non-zinc glyoxalase I from *Escherichia coli*: evidence for optimal activation by nickel ions. *Biochemistry* **37**, 8754–8763.
  - 27 Dai Y, Wensink PC & Abeles RH (1999) One protein, two enzymes. *J Biol Chem* **274**, 1193–1195.
  - 28 Youn HD, Kim EJ, Roe JH, Hah YC & Kang SO (1996) A novel nickel-containing superoxide dismutase from *Streptomyces* Spp. *Biochem J* **318**, 889–896.
  - 29 Youn HD, Youn H, Lee JW, Yim YI, Lee JK, Hah YC *et al.* (1996) Unique isozymes of superoxide dismutase in *Streptomyces griseus*. *Arch Biochem Biophys* **334**, 341–348.
  - 30 Kim FJ, Kim HP, Hah YC & Roe JH (1996) Differential expression of superoxide dismutases containing Ni and Fe/Zn in *Streptomyces coelicolor*. *Eur J Biochem* **241**, 178–185.
  - 31 Volbeda A, Charon MH, Piras C, Hatchikian EC, Frey M & Fontecilla-Camps JC (1995) Crystal structure of the nickel-iron hydrogenase from *Desulfovibrio gigas*. *Nature* **373**, 580–587.
  - 32 Armstrong FA & Albracht SPJ (2005) [NiFe]-hydrogenases: spectroscopic and electrochemical definition of reactions and intermediates. *Philos Trans A Math Phys Eng Sci* **363**, 937–954.
  - 33 Thauer RK, Kaster AK, Goenrich M, Schick M, Hiromoto T & Shima S (2010) Hydrogenases from methanogenic archaea, nickel, a novel cofactor, and H<sub>2</sub> storage. *Annu Rev Biochem* **79**, 507–536.
  - 34 Nitschke W, McGlynn SE, Milner-white EJ & Russell MJ (2013) On the antiquity of metalloenzymes and their substrates in bioenergetics. *Biochim Biophys Acta* **1827**, 871–881.
  - 35 Ogata H, Lubitz W & Higuchi Y (2016) Structure and function of [NiFe] hydrogenases. *J Biochem* **160**, 251–258.
  - 36 Harrison DJ, Lough AJ & Fekl U (2018) A new structural model for NiFe hydrogenases: an unsaturated analogue of a classic hydrogenase model leads to more enzymes-like Ni-Fe distance and interplanar fold. *Acta Crystallogr Sect E Crystallogr Commun* **74**, 1222–1226.
  - 37 Dobbek H, Svetlitchnyi V, Gremer L, Huber R & Meyer O (2001) Crystal structure of a carbon monoxide dehydrogenase reveals a [Ni-4-Fe-5S] cluster. *Science* **293**, 1281–1285.
  - 38 Jeoung JH & Dobbek H (2007) Carbon dioxide activation at the Ni,Fe-cluster of anaerobic carbon monoxide dehydrogenase. *Science* **318**, 1461–1464.
  - 39 Can M, Armstrong FA & Ragsdale SW (2014) Structure, function, and mechanism of the nickel metalloenzymes, CO dehydrogenase, and acetyl-CoA synthase. *Chem Rev* **114**, 4149–4174.
  - 40 Can M, Giles LJ, Ragsdale SW & Sarangi R (2017) X-ray absorption spectroscopy reveals an organometallic Ni-C bond in the CO-treated form of acetyl-CoA synthase. *Biochemistry* **56**, 1248–1260.
  - 41 Biester A, Grahame DA & Drennan CL (2024) Capturing a methanogenic carbon monoxide dehydrogenase/acetyl-CoA synthase complex via cryogenic electron microscopy. *Proc Natl Acad Sci U S A* **121**, e2410995121.
  - 42 Svetlitchnyi V, Dobbek H, Neyer-Klaucke W, Meins T, Thiele B, Römer P *et al.* (2004) A functional Ni-Ni-[4Fe-4S] cluster in the monomeric acetyl-CoA synthase from *Carboxydotherrmus hydrogenofomans*. *Proc Natl Acad Sci U S A* **101**, 446–451.
  - 43 Rospert S, Böcher R, Albracht SPJ & Thauer RK (1991) Methyl-coenzyme M reductase preparations with high specific activity from H<sub>2</sub> preincubated cells

- of *Methanobacterium thermoautotrophicum*. *FEBS Lett* **291**, 371–375.
- 44 Goubeaud M, Schreiner G & Thauer RK (1997) Purified methyl-coenzyme-M reductase is activated when the enzyme-bound coenzyme F<sub>430</sub> is reduced to the nickel(I) oxidation state by titanium(III) citrate. *Eur J Biochem* **243**, 110–114.
- 45 Goenrich M, Mahler F, Duin EC, Bauer C, Jaun B & Thauer RK (2004) Probing the reactivity of Ni in the active site of methyl-coenzyme M reductase with substrate analogues. *J Biol Inorg Chem* **9**, 691–705.
- 46 Wongnate T, Sliwa D, Ginovska B, Smith D, Wolf MW, Lehnert N *et al.* (2016) The radical mechanism of biological methane synthesis by methylcoenzyme M reductase. *Science* **352**, 953–958.
- 47 Thauer RK (2019) Methyl (alkyl)-coenzyme m reductases: nickel F-430-containing enzymes involved in anaerobic methane formation and in anaerobic oxidation of methane or of short chain alkanes. *Biochemistry* **58**, 5198–5220.
- 48 Ueno Y, Yamada K, Yoshida N, Maruyama S & Isozaki Y (2006) Evidence from fluid inclusions for microbial methanogenesis in the early archaean era. *Nature* **440**, 516–519.
- 49 Martin WF, Baross J, Kelley D & Russell MJ (2008) Hydrothermal vents and the origin of life. *Nat Rev Microbiol* **6**, 805–814.
- 50 Shima S, Huang G, Wagner T & Ermler U (2020) Structural basis of hydrogenotrophic methanogenesis. *Annu Rev Microbiol* **74**, 713–733.
- 51 Huber C & Wächtershäuser G (1997) Activated acetic acid by carbon fixation on (Fe,Ni)S under primordial conditions. *Science* **276**, 245–247.
- 52 Roldan A, Hollingsworth N, Roffey A, Islam HU, Goodall JBM, Catlow CRA *et al.* (2015) Bio-inspired CO<sub>2</sub> conversion by iron sulfide catalysts under sustainable conditions. *Chem Commun* **51**, 7501–7504.
- 53 Kitadai N, Nakamura R, Yamamoto M, Takai K, Li Y, Yamaguchi A *et al.* (2018) Geoelectrochemical CO production: implications for the autotrophic origin of life. *Sci Adv* **4**, eaao7265.
- 54 Kitadai N, Nakamura R, Yamamoto M, Okada S, Takahagi W, Nakano Y *et al.* (2021) Thioester synthesis through geoelectrochemical CO<sub>2</sub> fixation on Ni sulfides. *Commun Chem* **4**, 37.
- 55 Kitadai N, Nakamura R, Yamamoto M, Takai K, Yoshida N & Oono Y (2019) Metals likely promoted protometabolism in early ocean alkaline hydrothermal systems. *Sci Adv* **5**, eaav7848.
- 56 Beyazay T, Belthe KS, Farès C, Preiner M, Moran J, Martin WF *et al.* (2023) Ambient temperature CO<sub>2</sub> fixation to pyruvate and subsequently to citramalate over iron and nickel nanoparticles. *Nat Commun* **14**, 570.
- 57 Mrnjavac N, Wimmer JLE, Brabender M, Schwander L & Martin WF (2023) The moon-forming impact and the autotrophic origin of life. *ChemPlusChem* **88**, e202300270.
- 58 Muchowska KB, Varma SJ, Chevallot-Beroux E, Lethuillier-Karl L, Li G & Moran J (2017) Metals promote sequences of the reverse Krebs cycle. *Nat Ecol Evol* **1**, 1716–1721.
- 59 Varma SJ, Muchowska KB, Chatelain P & Moran J (2018) Native iron reduces CO<sub>2</sub> to intermediates and end-products of the acetyl-CoA pathway. *Nat Ecol Evol* **2**, 1019–1024.
- 60 Preiner M, Igarashi K, Muchowska KB, Yu M, Varma SJ, Kleinermanns K, Nobu MK, Kamagata Y, Tüysüz H, Moran J *et al.* (2020) A hydrogen-dependent geochemical analogue of primordial carbon and energy metabolism. *Nat Ecol Evol* **4**, 534–542.
- 61 Belthe KS, Beyazay T, Ochoa-Hernández C, Miyazaki R, Foppa L, Martin WF & Tüysüz H (2022) Effects of silica modification (Mg, Al, Ca, Ti, and Zr) on supported cobalt catalysts for H<sub>2</sub>-dependent CO<sub>2</sub> reduction to metabolic intermediates. *J Am Chem Soc* **144**, 21232–21243.
- 62 Beyazay T, Ochoa-Hernández C, Song Y, Belthe KS, Martin WF & Tüysüz H (2023) Influence of composition of nickel-iron nanoparticles for abiotic CO<sub>2</sub> conversion to early prebiotic organics. *Angew Chem Int Ed* **62**, e202218189.
- 63 Belthe KS, Martin WF & Tüysüz H (2024) Synergistic effects of silica-supported iron-cobalt catalysts for CO<sub>2</sub> reduction to prebiotic organics. *ChemCatChem* **16**, e202301218.
- 64 Kaur H, Rauscher S, Werner E, Song Y, Yi J, Kazöne W, Martin WF, Tüysüz H & Moran J (2024) A prebiotic Krebs cycle analog generates amino acids with H<sub>2</sub> and NH<sub>3</sub> over nickel. *Chem* **10**, 1528–1540.
- 65 Henriques Pereira DP, Leethaus J, Beyazay T, do Nascimento Vieira A, Kleinermanns K, Tüysüz H, Martin WF & Preiner M (2022) Role of geochemical protoenzymes (geozymes) in primordial metabolism: specific abiotic hydride transfer by metals to the biological redox cofactor NAD<sup>+</sup>. *FEBS J* **289**, 3148–3162.
- 66 Henriques Pereira DP, Xie X, Stewart SV, Subrati Z, Beyazay T, Paczia N, Belz J, Volz K, Erastova V, Tüysüz H *et al.* (2025) Reduction of NAD and NMN on mineral surfaces with H<sub>2</sub> reveals a functional role for the AMP moiety in a prebiotic context. *Commun Chem* **8**, 318.
- 67 Schlikker ML, Brabender M, Schwander L, Garcia Garcia C, Burmeister M, Metzger S, Moran J & Martin WF (2025) Conversion of pyridoxal to pyridoxamine with NH<sub>3</sub> and H<sub>2</sub> on nickel generates a protometabolic nitrogen shuttle under serpentinizing conditions. *FEBS J* **292**, 3041–3055.

- 68 Bard AJ, Parsons R & Jordan J (1985) Standard Potentials in Aqueous Solution. 1st edn. Routledge, New York.
- 69 Brabender M, Henriques Pereira DP, Mrnjavac N, Schlikker ML, Kimura ZI, Sucharitakul J, Kleinermanns K, Tüysüz H, Buckel W, Preiner M *et al.* (2024) Ferredoxin reduction by hydrogen with iron functions as an evolutionary precursor of flavin-based electron bifurcation. *Proc Natl Acad Sci U S A* **121**, e2318969121.
- 70 Chamberlain JA, McLeod CR, Traill RJ & Lachance GR (1965) Native metals in the muskox intrusion. *Can J Earth Sci* **2**, 188–215.
- 71 Russell MJ, Hall AJ & Martin WF (2010) Serpentinization as a source of energy at the origin of life. *Geobiology* **8**, 355–371.
- 72 Schwarzenbach EM, Vrijmoed JC, Engelmann JM, Liesegang M, Wiechert U, Rohne R & Plümper O (2021) Sulfide dissolution and awaruite formation in continental serpentinization environments and its implications to supporting life. *J Geophys Res Solid Earth* **126**, e2021JB021758.
- 73 Horita J & Berndt ME (1999) Abiogenic methane formation and isotopic fractionation under hydrothermal conditions. *Science* **285**, 1055–1057.
- 74 Etiope G & Sherwood Lollar B (2013) Abiotic methane on earth. *Rev Geophys* **51**, 276–299.
- 75 Mrnjavac N, Schwander L, Brabender M & Martin WF (2024) Chemical antiquity in metabolism. *Acc Chem Res* **57**, 2267–2278.
- 76 Song Y & Tüysüz H (2024) CO<sub>2</sub> fixation to prebiotic intermediates over heterogeneous catalysts. *Acc Chem Res* **57**, 2038–2047.
- 77 Diekert G & Thauer RK (1980) The effect of nickel on carbon monoxide dehydrogenase formation in *Clostridium thermoaceticum* and *Clostridium formicoaceticum*. *FEMS Microbiol Lett* **7**, 187–189.
- 78 Adkins H & Cramer HI (1930) The use of nickel as a catalyst for hydrogenation. *J Am Chem Soc* **52**, 4349–4358.
- 79 Rana S, Masli N, Monder DS & Chatterjee A (2022) Hydriding pathway for Ni nanoparticles: computational characterization provides insights into the nanoparticle size and facet effect on layer-by-layer subsurface hydride formation. *Comput Mater Sci* **210**, 111482.
- 80 Schwander L, Brabender M, Mrnjavac N, Wimmer JLE, Preiner M & Martin WF (2023) Serpentinization as the source of energy, electrons, organics, catalysts, nutrients and pH gradients for the origin of LUCA and life. *Front Microbiol* **14**, 1257597.
- 81 Thauer RK, Kaster AK, Seedorf H, Buckel W & Hedderich R (2008) Methanogenic archaea: ecologically relevant differences in energy conservation. *Nat Rev Microbiol* **6**, 579–591.
- 82 Munoz L & Philips J (2023) No acetogen is equal: strongly different H<sub>2</sub> thresholds reflect diverse bioenergetics in acetogenic bacteria. *Environ Microbiol* **25**, 2032–2040.
- 83 Hodgkin DMC (1965) The structure of the corrin nucleus from X-ray analysis. *Proc R Soc Lond A Math Phys Eng Sci* **288**, 294–305.
- 84 Marques HM & Brown KL (1999) The structure of cobalt corrinoids based on molecular mechanics and NOE-restrained molecular mechanics and dynamics simulations. *Coord Chem Rev* **190–192**, 127–153.
- 85 Johnson JL, Hainline BE & Rajagopalan KV (1980) Characterization of the molybdenum cofactor of sulfide oxidase, xanthine oxidase, and nitrate reductase. Identification of a pteridine as a structural component. *J Biol Chem* **255**, 1783–1786.
- 86 Johnson JL & Rajagopalan KV (1982) Structural and metabolic relationship between the molybdenum cofactor and urothione. *Proc Natl Acad Sci U S A* **79**, 6856–6860.
- 87 Buurman G, Shima S & Thauer RK (2000) The metal-free hydrogenase from methanogenic archaea: evidence for a bound cofactor. *FEBS Lett* **485**, 200–204.
- 88 Shima S, Lyon EJ, Sordel-Klippert M, Kauß M, Kahnt J, Thauer RK *et al.* (2004) The cofactor of the iron-sulfur cluster free hydrogenase Hmd: structure of the light-inactivation product. *Angew Chem Int Ed* **43**, 2547–2551.
- 89 Gatreddi S, Chatterjee S, Turmo A, Hu J & Hausinger RP (2024) A structural view of nickel-pincer nucleotide cofactor-related biochemistry. *Crit Rev Biochem Mol Biol* **59**, 402–417.
- 90 Desguin B, Zhang T, Soumillon P, Hols P, Hu J & Hausinger RP (2015) A tethered niacin-derived pincer complex with a nickel-carbon bond in lactate racemase. *Science* **349**, 66–69.
- 91 Boyd ES, Amenabar MJ, Poudel S & Templeton AS (2020) Bioenergetic constraints on the origin of autotrophic metabolism. *Philos Trans R Soc Lond A Math Phys Eng Sci* **379**, 20190151.
- 92 Suzuki S, Ishii S, Hoshino T, Rietze A, Tenney A, Morrill PL, Inagaki F, Kuenen JG & Nealson KH (2017) Unusual metabolic diversity of hyperalkaliphilic microbial communities associated with subterranean serpentinization at the cedars. *ISME J* **11**, 1584–1598.
- 93 Colman DR, Kraus EA, Thieringer PH, Rempfert K, Templeton AS, Spear JR *et al.* (2022) Deep-branching acetogens in serpentinized subsurface fluids of Oman. *Proc Natl Acad Sci U S A* **119**, e2206845119.
- 94 Nobu MK, Nakai R, Tamazawa S, Mori H, Toyoda A, Ijiri A *et al.* (2023) Unique H<sub>2</sub>-utilizing lithotrophy in serpentinite-hosted systems. *ISME J* **17**, 95–104.
- 95 Komesu A, Marins Martínez PH, Lunelli BH, Oliveira J, Wolf Maclel MR & Maclel Filho R (2017)

- Study of lactic acid thermal behavior using thermoanalytical techniques. *J Chem* **2017**, 4149592.
- 96 Beverskog B & Puigdomenech I (1997) Revised Pourbaix diagrams for nickel at 25–300 °C. *Corros Sci* **39**, 969–980.
- 97 Mrnjavac N, Hoffmann NK, Schlikker ML, Burmeister M, Schwander L, Garcia Garcia C, Brabender M, Steel M, Huson DH, Metzger S *et al.* (2025) Gradual assembly of metabolism at a phosphorylating hydrothermal vent. *arXiv*, arXiv2510:08410.
- 98 Sleep NH, Meibom A, Fridriksson T, Coleman RG & Bird DK (2004) H<sub>2</sub>-rich fluids from serpentinization: geochemical and biotic implications. *Proc Natl Acad Sci U S A* **101**, 12818–12823.
- 99 McCollom TM & Seewald JS (2013) Serpentinites, hydrogen, and life. *Elements* **9**, 129–134.
- 100 Sinton JM (1976) Compositional relationships of Fe-Ni alloy and coexisting phases in serpentinite, Red Mountain, New Zealand. *Mineral Mag* **40**, 792–794.
- 101 Lorand JP (1987) Cu-Fe-Ni-S mineral assemblages in upper-mantle peridotites from the Table Mountain and blow-me-down Mountain ophiolite massifs (bay of islands area, Newfoundland): their relationships with fluids and silicate melts. *Lithos* **20**, 59–76.
- 102 Klein F, Bach W, Jöns N, McCollom TM, Moskowitz B & Berquó T (2009) Iron partitioning and hydrogen generation during serpentinization of abyssal peridotites from 15° N of the mid-Atlantic ridge. *Geochim Cosmochim Acta* **73**, 6868–6893.
- 103 Tamblyn R & Hermann J (2023) Geological evidence for high H<sub>2</sub> production from komatiites in the archaean. *Nat Geosci* **16**, 1194–1199.
- 104 Lawley CJM, Petts DC, Jackson SE, Zagorevski A, Pearson DG, Kjarsgaard BA *et al.* (2020) Precious metal mobility during serpentinization and breakdown of base metal sulphide. *Lithos* **354–355**, 105278.
- 105 Kutyrev A, Kamenetsky VS, Kontonikas-Charos A, Savelyev DP, Yakich TY, Belousov IA *et al.* (2023) Behaviour of platinum-group elements during hydrous metamorphism: constraints from awaruite (Ni<sub>3</sub>Fe) mineralization. *Lithosphere* **2023**, lithosphere2023126.
- 106 Rauscher SA & Moran J (2022) Hydrogen drives part of the reverse Krebs cycle under metal or meteorite catalysis. *Angew Chem Int Ed* **61**, e202212932.
- 107 Lancaster CRD, Kröger A, Auer M & Michel H (1999) Structure of fumarate reductase from *Wolinella suxinogenes* at 2.2 Å resolution. *Nature* **402**, 377–385.
- 108 Boyington JC, Gladyshev VN, Khangulov SV, Stadtman TC & Sun PD (1997) Crystal structure of formate dehydrogenase H: catalysis involving Mo, molybdopterin, selenocysteine, and an Fe<sub>4</sub>S<sub>4</sub> cluster. *Science* **275**, 1305–1308.
- 109 Buckel W & Thauer RK (2013) Energy conservation via electron bifurcating ferredoxin reduction and proton/Na(+) translocating ferredoxin oxidation. *Biochim Biophys Acta* **1827**, 94–113.
- 110 Kaster AK, Moll J, Parey K & Thauer RK (2011) Coupling of ferredoxin and heterodisulfide reduction via electron bifurcation in hydrogenotrophic methanogenic archaea. *Proc Natl Acad Sci U S A* **108**, 2981–2986.
- 111 Jensen RA (1976) Enzyme recruitment in evolution of new function. *Annu Rev Microbiol* **30**, 409–425.
- 112 Khersonsky O & Tawfik DS (2010) Enzyme promiscuity: a mechanistic and evolutionary perspective. *Annu Rev Microbiol* **79**, 471–505.

## Supporting information

Additional supporting information may be found online in the Supporting Information section at the end of the article.

**Table S1.** Raw data Fig. 1. Raw data of product concentrations with and without nickel and ammonium chloride. Initial concentrations were 20 mM pyruvate and 200 mM ammonium chloride. Ni-SiO<sub>2</sub>/Al<sub>2</sub>O<sub>3</sub> (1 mmol of Ni atoms) was added as solid phase powder in a total reaction volume of 1.5 mL. The reaction was performed under a 5 bar Ar atmosphere, initial pH 11 with KOH, the reaction time was 18 h at 100 °C. No H<sub>2</sub> was added. Reactions were performed in triplicates.

**Table S2.** Raw data Fig. 2. Raw data of product concentrations at different pH values. Initial concentrations were 20 mM of pyruvate. Ni-SiO<sub>2</sub>/Al<sub>2</sub>O<sub>3</sub> (1 mmol of Ni atoms) was added as solid phase powder in a total reaction volume of 1.5 mL. The pH was set to 7, 8, 9, 10, and 11 with KOH, respectively, and the reaction time was set to 2 h. The reaction was performed under a 5 bar Ar atmosphere. No H<sub>2</sub> was added. Each dot represents a single measurement. Dots positioned on the X axis represent measurements where no concentration could be detected. Reactions were performed in triplicates.

**Table S3.** Raw data Fig. 3. Raw data of product concentrations with different temperature and time conditions. Initial concentrations were 20 mM of pyruvate. Ni-SiO<sub>2</sub>/Al<sub>2</sub>O<sub>3</sub> (1 mmol of Ni atoms) was added as solid phase powder in a total reaction volume of 1.5 mL. The reaction time was 1 h (B), 2 h (B), 4 h (C), and 18 h (D), respectively. Temperature was 25, 40, 60, 80, and 100 °C. The pH was set to 9 with KOH. The reaction was performed under a 5 bar Ar atmosphere. No H<sub>2</sub> was added. Reactions were performed in triplicates.

**Table S4.** Raw data Fig. 4. Raw data of product concentrations with different catalysts. Pyruvate

concentration was set to 20 mM. The catalysts (Ni-SiO<sub>2</sub>/Al<sub>2</sub>O<sub>3</sub>, Nano nickel powder, micro nickel powder, SiO<sub>2</sub>/Al<sub>2</sub>O<sub>3</sub>) were added as 1 mmol of Ni atoms of undissolved solid phase powder in a total reaction volume of 1.5 mL. The reaction was performed at 100 °C, under a 5 bar argon atmosphere, pH was set to 9 with KOH. No H<sub>2</sub> was added. The reaction time was set to 2 h (A), and 18 h (B). Each reaction was performed in triplicates.

**Table S5.** Raw data Fig. 5. Raw data of product concentrations with different catalyst concentrations. Initial concentrations were 20 mM of pyruvate. Ni-SiO<sub>2</sub>/Al<sub>2</sub>O<sub>3</sub> was added as solid phase at a concentration of 0.05, 0.11, 0.22, 0.33, 0.66, 1, and 1.5 mmol of Ni atoms, respectively. The pH was 9 (KOH), and the reaction was performed at 2 h at 100 °C, under a 5 bar Ar atmosphere. No H<sub>2</sub> was added. Each reaction was performed in triplicates.

**Table S6.** Raw data Fig. 6. Raw data of ketone and double bond reduction product concentrations. Educt concentration was set to 20 mM. Ni-SiO<sub>2</sub>/Al<sub>2</sub>O<sub>3</sub> (1 mmol of Ni atoms) was added as solid phase pow-

der in a total reaction volume of 1.5 mL. The reaction time was set to 2 h at 100 °C, and pH was set to 9 with KOH. The reaction was performed under a 5 bar Ar atmosphere. No H<sub>2</sub> was added. Each reaction was performed in triplicates. (A) Succinate synthesis from fumarate. (B) 2-Hydroxyglutarate synthesis from 2-oxoglutarate. (C) 2-Hydroxyisocaproate synthesis from 4-methyl-2-oxopentanoate. (D) 2-Hydroxy-3-methylvalerate synthesis from 3-methyl-2-oxopentanoate.

**Table S7.** Raw data Fig. 7. Raw data of reductive amination product concentrations. Initial concentrations were 20 mM of each respective educt and 200 mM ammonium chloride. Ni-SiO<sub>2</sub>/Al<sub>2</sub>O<sub>3</sub> (1 mmol of Ni atoms) was added as solid phase powder in a total reaction volume of 1.5 mL. The reaction was performed under a 5 bar Ar atmosphere, initial pH 11 with KOH, the reaction was set at 72 h and 100 °C. No H<sub>2</sub> was added. Reactions were performed in triplicates. (A) Leucine synthesis from 4-methyl-2-oxopentanoate. (B) Isoleucine synthesis from 3-methyl-2-oxopentanoate. (C) 5-Oxoproline synthesis from 2-oxoglutarate.